

# PROCEEDINGS OF SPIE

[SPIDigitalLibrary.org/conference-proceedings-of-spie](https://SPIDigitalLibrary.org/conference-proceedings-of-spie)

## Generalized Brewster effect in aluminum-doped ZnO nanopillars

Chatterjee, Sharmistha, Shkondin, Evgeniy, Takayama, Osamu, Lavrinenko, Andrei, Hinczewski, Michael, et al.

Sharmistha Chatterjee, Evgeniy Shkondin, Osamu Takayama, Andrei V. Lavrinenko, Michael Hinczewski, Giuseppe Strangi, "Generalized Brewster effect in aluminum-doped ZnO nanopillars," Proc. SPIE 11345, Nanophotonics VIII, 1134524 (1 April 2020); doi: 10.1117/12.2554559

**SPIE.**

Event: SPIE Photonics Europe, 2020, Online Only

# Generalized Brewster Effect in Aluminum-doped ZnO Nanopillars

Sharmistha Chatterjee, <sup>†, ‡</sup> Evgeniy Shkondin, <sup>§</sup> Osamu Takayama, <sup>§</sup> Andrei V. Lavrinenko, <sup>§</sup> Michael Hinczewski, <sup>‡</sup> and Giuseppe Strangi <sup>\*, ‡, †</sup>

<sup>†</sup> CNR-NANOTEC Istituto di Nanotecnologia and Department of Physics, University of Calabria, 87036 Rende, Italy.

<sup>‡</sup> Department of Physics, Case Western Reserve University, 10600 Euclid Avenue, Cleveland, OH 44106, USA.

<sup>§</sup> DTU Nanolab - National Center for Micro- and Nanofabrication, Technical University of Denmark, Ørstedsgade 347, DK-2800 Lyngby, Denmark.

<sup>§</sup> DTU Fotonik - Department of Photonics Engineering, Technical University of Denmark, Ørstedsgade 343, DK-2800 Lyngby, Denmark.

\* E-mail: gxs284@case.edu

Phone: (216) 368 6918

**ABSTRACT:** Generalized Brewster effect is a phenomenon where light of both TE (S-) and TM (P-) polarization transmit through a surface with no reflection for a particular incident angle. Generalized Brewster angle (GBA) in visible and near-infrared (NIR) wavelength region is very useful in many scientific and technical areas of applications. However, it is very rare to find a material having this effect as it demands both dielectric and magnetic response in that wavelength range and usually magnetic response is extremely weak in the optical wavelengths. Here we demonstrate the GBA effect of an anisotropic material composed of highly ordered high aspect ratio aluminium doped zinc oxide (AZO) nanopillar arrays. Along with the experimental demonstration, we also provide a proper numerical analysis to investigate the origin of this effect in the pillar array system which will be useful for many conventional as well as new applications in photonics including protein sensing.

**KEYWORDS:** Zinc Oxide, Transparent Conductive Oxide, AZO, Brewster Angle, Metamaterial, Metasurface.

**INTRODUCTION:** Brewster angle,  $\theta_B$ , is a particular incidence angle at which light of certain polarization can transmit perfectly through a dielectric surface without reflection <sup>[1-2]</sup>. Therefore, the reflection of the unpolarized light incident at  $\theta_B$  is a perfectly polarized light, as well as the transmitted one. Brewster's angle is also known as the polarizing angle as the reflected light from a surface at this angle is completely a polarized light which has polarization perpendicular to the plane of incidence. Brewster showed in his popular Brewster law that  $\theta_B$  is a function of the refractive indices of the material used. Here it is worth mentioning that, as the refractive index of a medium depends on the wavelength of the incident light, thus  $\theta_B$  also varies with the chosen wavelength. The Brewster angle is useful for many practical applications, such as polarized sunglasses for reducing glare of sun reflecting off horizontal surfaces, polarizing filter cameras, holograms, Brewster angle prisms to minimize reflection losses for laser physics <sup>[3]</sup>, Brewster

windows for gas lasers, cavity mirrors, high-performance terahertz modulators<sup>[4]</sup>, and Brewster angle microscopes for the study of surface science<sup>[5-6]</sup>.

For all the above discussion of  $\theta_B$  we have assumed that the reflection is taking place from a homogeneous, non-magnetic, achiral, and isotropic material. Generally, Brewster angle effect occurs either for s-polarized light or for p-polarized light. For a normal dielectric material, the Brewster phenomenon of p-polarized light is a common event. On the other hand,  $\theta_B$  for s-polarized light generally can be seen in a magnetic material with permeability  $\mu \neq 1$  and it is quite rare at visible and NIR frequencies as their magnetic response is extremely weak ( $\mu \approx 1$ ) in that wavelength range. GBA is the incidence angle at which the Brewster angle effect for both the polarization takes place. In other words, at the particular incidence angle, reflection for p- as well as s-polarized light vanishes<sup>[1-2]</sup>. For the GBA effect to occur in a particular material, both the p- and s-polarization Brewster angle effect is needed which is only possible when the material has dielectric and magnetic response. Therefore, it is hard to meet the requirement of magnetic response at visible and NIR wavelength range along with the dielectric response in a material, making it difficult to find GBA effect in a material in that wavelength region. For some magnetic materials, although one can see GBA effect, yet  $\theta_B$  for s-polarized light ( $\theta_B^{s-pol}$ ) is not same as the  $\theta_B$  for the p-polarized light ( $\theta_B^{p-pol}$ ) for non-normal incidence angle<sup>[7]</sup>. Therefore, the only necessary and sufficient condition for GBA effect is that the vector resultant radiation field should vanish in the reflection due to the total destructive interference of the magnetic and electric dipoles of the magnetic material at  $\theta_B^{s,p-pol}$ <sup>[8]</sup>. For normal magnetic materials, the Brewster's angle exists only for either s- or p-polarization, which is controlled by the relative strengths of the dielectric permittivity and magnetic permeability<sup>[9]</sup>. This fact is very useful for the explanation of generalized Brewster angles in specific systems, for example, in dielectric metasurfaces<sup>[10]</sup>.

The generalized Brewster angle effect has been observed experimentally in microwave region using the split-ring resonators<sup>[11-12]</sup>. The GBA effect was also experimentally demonstrated in anisotropic material<sup>[13]</sup>, graphene combined with thin film absorber<sup>[3]</sup>, chiral materials<sup>[14]</sup>, and a multilayer structure<sup>[15]</sup>. In addition, s-polarized Brewster effect was observed in stratified metal-dielectric metamaterial,<sup>[16]</sup> graphene layer<sup>[3, 17]</sup>, and all-dielectric metamaterials at the optical frequency<sup>[18]</sup>. Metamaterials, with negative permeability and thus with a magnetic response, support the GBA effect<sup>[19-21]</sup>. However, those works did not show the GBA effect of both polarizations in the reflected light, especially for the s-polarized light<sup>[18]</sup>. There, unequal reflection for p- and s-polarized light was observed, which is quite normal for non-magnetic material, and therefore it cannot be considered as a true generalized Brewster effect as this is obvious according to the Fresnel equations.

Here we experimentally demonstrate the presence of the generalized Brewster angle effect in the high aspect ratio highly ordered aluminium doped ZnO (AZO) solid pillar structures. The high aspect ratio AZO pillars were fabricated by a combination of advanced deep ultraviolet (DUV) lithography, deep reactive ion etching (DRIE), and atomic layer deposition (ALD) techniques<sup>[22]</sup>. The diameter and height of these pillars are 300 nm and 2  $\mu\text{m}$ , respectively, and a pitch of 400 nm and 500 nm is maintained over 1 x 1  $\text{cm}^2$  area. For these structures, air acts as the host material and all these nanopillars are standing over a 200 nm thick  $\text{SiO}_2$  layer deposited on a Si wafer. These AZO structures satisfy both the p- and s-polarization Brewster condition experimentally at wavelengths in the NIR region. The GBA wavelength can also

be tuned by the angle of incidence which adds one more advantage to these structures. Therefore, the GBA effect along with the strong near field localization capability makes these high aspect ratio AZO nanostructures useful for many applications, such as low-power ultrafast optical switches, perfect light absorbers, Brewster windows in gas lasers including protein sensing. In order to deeply understand the cause of the GBA effect of the AZO nanopillar array system, numerical investigations have also been performed here. The following paragraphs describe the design and the nanofabrication process of the nanopillars array system along with the numerical study and the experimental results which supports the GBA effect of the array structures.

## EXPERIMENTAL SECTION:

**Fabrication of AZO Nanopillars:** The home-made SOI (silicon-on-insulator) substrates has been prepared by thermally oxidizing the <100> Si wafers to the thickness of 200 nm and depositing 2  $\mu\text{m}$  amorphous Si by LPCVD (Low pressure chemical vapour deposition). Deep UV lithography was used to define square lattice patterns of photoresist on SOI substrates. Deep reactive ion etching (DRIE) was implemented with a standard Bosch process<sup>[23]</sup> in order to etch a Si template into the 2  $\mu\text{m}$ -deep air hole arrays, which was cleaned in  $\text{N}_2/\text{O}_2$  plasma to remove remaining resist and other organic contaminants. Then, the silicon templates were coated by AZO (using trimethylaluminum, diethylzinc, and water as precursors) by means of atomic layer deposition (ALD),<sup>[24]</sup> until the air holes were filled entirely. For the final step, the AZO filling needs to be isolated, and for that purpose, the samples were subjected to  $\text{Ar}^+$  sputtering for removal of the top AZO layer and exposing the silicon template. Afterwards, the silicon matrix in-between cavities coated with AZO, has been removed using  $\text{SF}_6$  plasma in conventional isotropic reactive ion etching process without interference with functional ALD material, resulting in the formation of AZO pillars as shown in Figure 1. The resulting AZO pillar structures on Si substrate have an intermediate thermally grown 200 nm silica layer (see Figure 1). The diameter, pitch, and height of the AZO pillars are 300 nm, 400 nm, and 2  $\mu\text{m}$ , respectively.<sup>[22]</sup> Here samples of AZO nanopillars arrays are also built with 500 nm pitch. In all the cases, the host material of the pillars is air and the array platforms are fabricated over  $1 \times 1 \text{ cm}^2$  area. The more detailed description of the fabrication method for different structures, such as, AZO trenches,<sup>[25-27]</sup> TiN trenches,<sup>[28]</sup> dielectric trenches,<sup>[29]</sup> coaxial tubes<sup>[30]</sup> can be found elsewhere. The optical properties of AZO films fabricated by ALD have been measured by spectroscopic ellipsometer for the wavelength range of interests.<sup>[22, 25]</sup>

**Ellipsometric Reflection Measurement:** A high-resolution variable-angle spectroscopic ellipsometry (SE) (J. A. Woollam Co., Inc., V-VASE) is used to experimentally measure all types of angular reflections and spectroscopic parameters. The low-power spectroscopic ellipsometer has high precision and it is also non-destructive. Thus SE is preferable for the optical characterization of these AZO pillar nanostructures. Here reflectivity  $R(\lambda, \phi)$  at different angle of incidence,  $\phi$ , in the wavelength range of  $\lambda = 300 - 3300 \text{ nm}$  is measured along with the measurement of spectroscopic parameters such as amplitude component, psi ( $\Psi$ ) and phase difference, delta ( $\Delta$ ). The maximum resolution of this ellipsometer is 0.03 nm but for our measurements 1 nm resolution is maintained throughout the experiments.

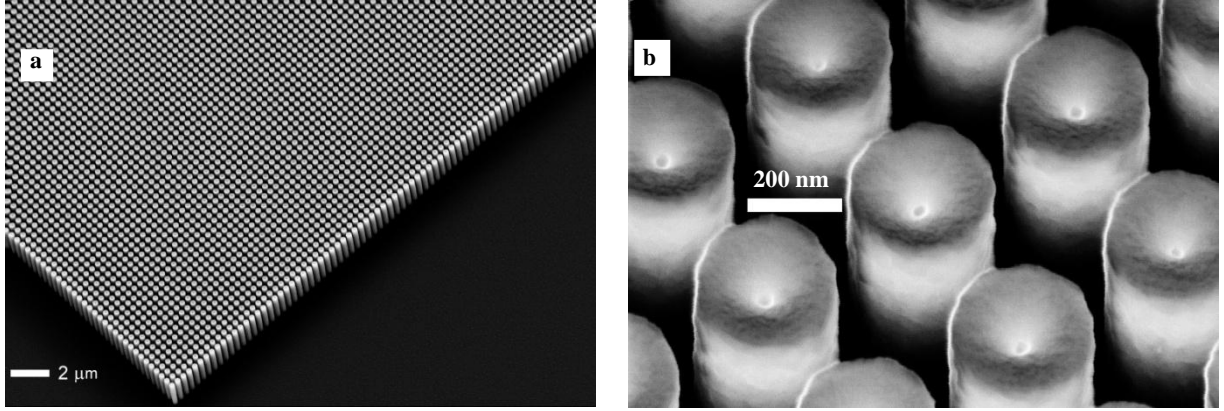


Figure 1: Scanning electron microscope (SEM) images of fabricated AZO (a, b) pillar array with a pitch of 400 nm, diameter of 300 nm, and height of 2 μm.

**Numerical Analysis:** In order to estimate the effective parallel ( $\epsilon_{\parallel}$ ) and perpendicular ( $\epsilon_{\perp}$ ) permittivities for the AZO nanopillar array system, we employed the following procedure. Spectroscopic parameters, psi ( $\Psi$ ) which is the amplitude component and delta ( $\Delta$ ) which is the phase difference were gathered for the entire system (AZO nanopillar, 200 nm SiO<sub>2</sub>, and Si substrate) in the wavelength range of 300 - 3300 nm using the SE. The complex reflectance ratio of the system measured by the SE follows the relation

$$\frac{r_p}{r_s} = \tan \Psi e^{i\Delta}$$

Where,  $\tan \Psi$  is the measurement of amplitude ratio upon reflection and  $e^{i\Delta}$  is connected to the phase shift. Here  $r_p$  and  $r_s$  is the normalized amplitude of the s- and p- polarized light respectively to their initial value after reflection. In order to model the ellipsometric data, we used a transfer matrix approach generalized for anisotropic metamaterials<sup>[31]</sup> based on Berreman matrices<sup>[32]</sup>. In order to apply this approach, we needed analytical forms for  $\epsilon_{\parallel}$  and  $\epsilon_{\perp}$ , which we derived from an effective medium approximation for a system of nanopillars surrounded by air<sup>[33]</sup>:

$$\epsilon_{\parallel} = \frac{1 - \rho + (1 + \rho)\epsilon_{AZO}}{1 + \rho + (1 - \rho)\epsilon_{AZO}}, \quad \epsilon_{\perp} = 1 - \rho + \rho\epsilon_{AZO} \quad (1)$$

Here  $\epsilon_{AZO}$  is the permittivity of AZO and  $\rho$  is the volume fraction of nanopillars in the layer ( $\rho = 0.44$  for the system with 400 nm pillar spacing, and  $\rho = 0.28$  for the one with 500 nm spacing). The final ingredient in the model is an effective medium approximation<sup>[34]</sup> for  $\epsilon_{AZO}$  based on a mixture with fraction  $\phi$  of Al (permittivity taken from Ref. [35]) and  $(1 - \phi)$  of ZnO. For the latter we use a permittivity based on the Wemple-DiDomenico model<sup>[36]</sup> with fitting parameters  $E_d$  and  $E_0$ . For the underlying SiO<sub>2</sub> layer and Si substrate, we use permittivities from Refs. [37] and [38], respectively. In total there are three fitting parameters ( $\phi$ ,  $E_d$ , and  $E_0$ ) which we optimize to most closely match the ellipsometric data. The best-fit results allow us to obtain  $\epsilon_{\parallel}$  and  $\epsilon_{\perp}$  through Eq. (1).

**Results and Discussions:** The optical characterization of AZO nanopillars array system of 400 nm and 500 nm pitch in square lattice with air host was conducted by the spectroscopic ellipsometer for both s- and p-polarized light which are shown in the Figure 2. The reflection measurements of AZO pillars with 500 nm pitch are shown for variable incident angles (15 deg to 25 deg by 5 deg) in panel (a) and (b) for p- and s- polarization respectively. Similarly, the reflection

measurements of AZO solid pillars with 400 nm pitch are shown for variable incident angles (35 deg to 45 deg by 5 deg) in Figure 2(c) and (d) for p- and s- polarization respectively. Here we can see that the AZO pillars of both type of pitches show GBA effect. For AZO samples at certain wavelength and angular range,  $R_p$  (reflection for p-polarized light) =  $R_s$  (reflection for s-polarized light) = 0. That particular wavelength is designated as the GBA wavelength and the corresponding angle as the GBA. For AZO pillars with 500 nm pitch, GBA effect is seen to occur around 1600 nm for the angular range of 15 deg to 25 deg. A clear blue shift of the GBA wavelength is seen for higher measurement angle. Similarly, for AZO pillars with 400 nm pitch, GBA effect occurs around 1500 nm for the angular range of 35 deg to 45 deg. In this case also a blue shift of the GBA wavelength is observed for higher measurement angle. It is worth mentioning that, compared to the case of AZO pillar arrays of 400 nm pitch, the AZO pillar sample with 500 nm pitch shows the GBA effect at smaller angular range and at higher wavelength range.

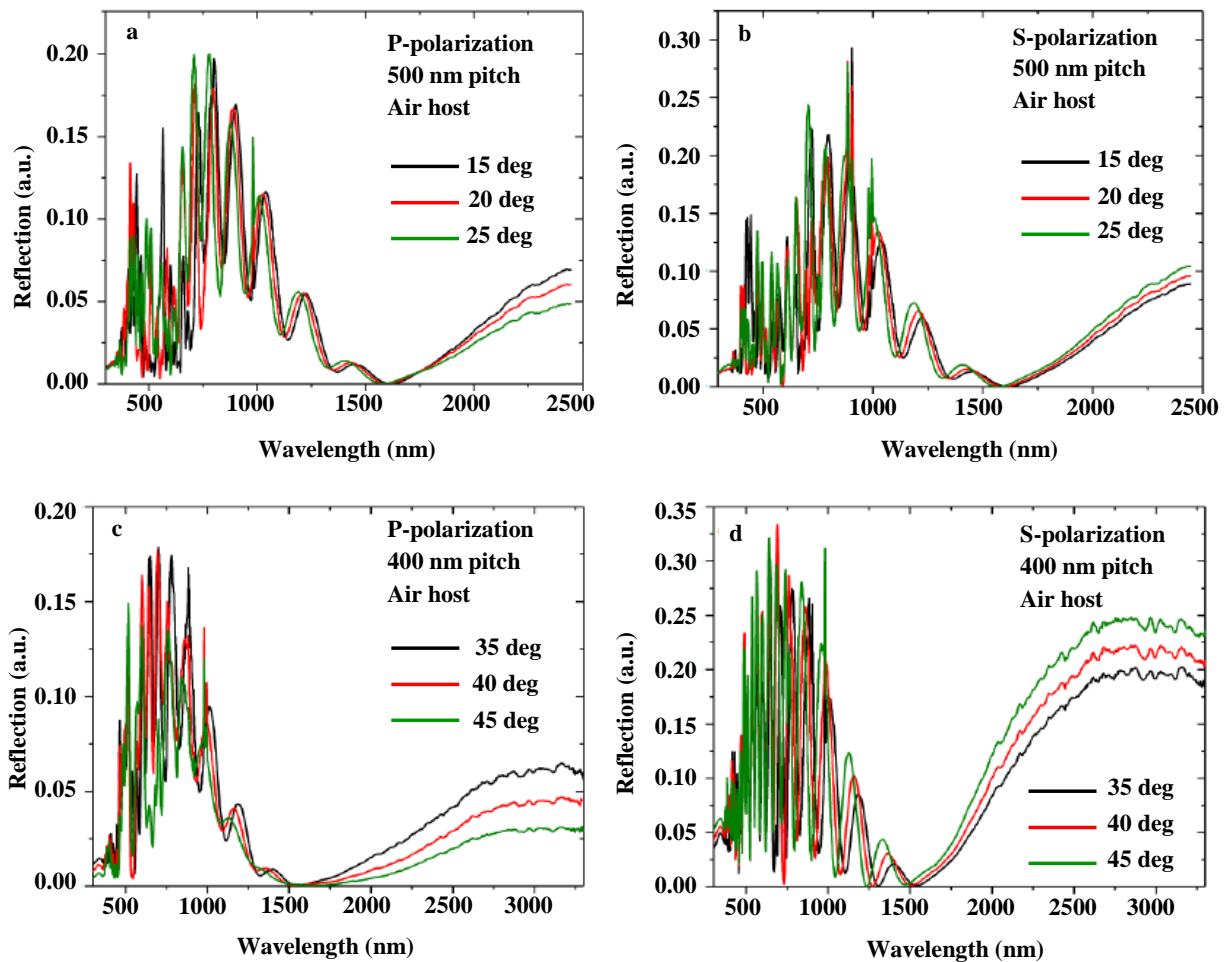


Figure 2. The reflection characteristics of the AZO nanopillars arrays with 500 nm pitch are shown for both (a) p-polarization and (b) s-polarization where the GBA effect is seen near 1600 nm and over an angular range of 15 deg to 25 deg. The reflection characteristics of the AZO nanopillars arrays with 400 nm pitch are shown for both (c) p-polarization and (d) s-polarization where the GBA effect is seen near 1500 nm and over an angular range of 35 deg to 45 deg. For both type of AZO pillar samples (with 400 nm and 500 nm pitch) air acts as the host material.

Now to proceed further to have a deeper insight of this GBA effect of the AZO pillar array system we focus only on the pillar arrays of 400 nm pitch which will also be applicable for the case of 500 nm pitch. The GBA effect and the wavelength at which that phenomenon occurs can be better understood from their spectroscopic parameter study, measured with the help of ellipsometer at those incident angles. Figure 3 shows both psi ( $\Psi$ ) and delta ( $\Delta$ ) characteristics at 35 deg, 40 deg and 45 deg incident angle measured with the help of spectroscopic ellipsometer.

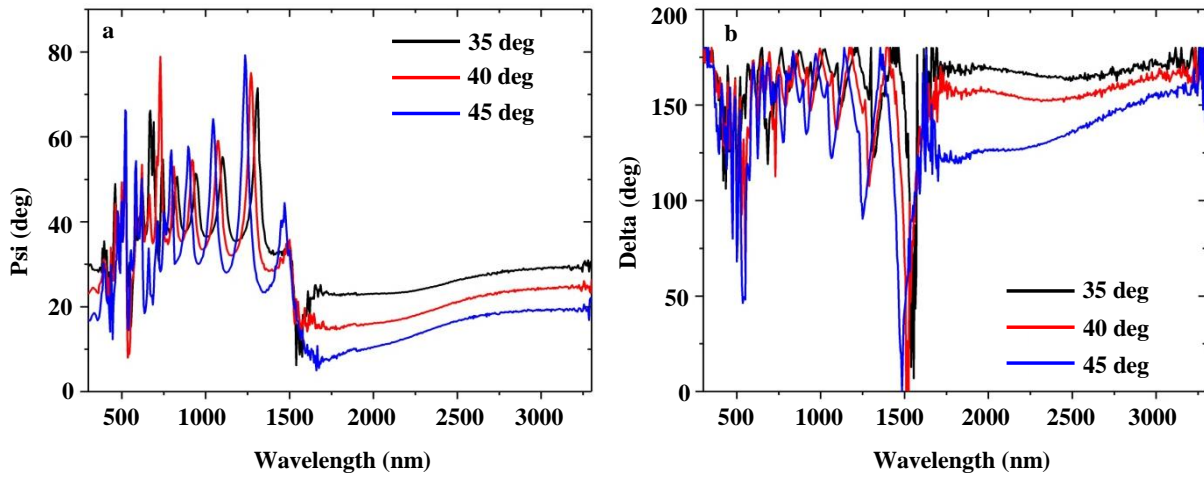


Figure 3. Spectroscopic parameters, (a) Psi ( $\Psi$ ) (b) Delta ( $\Delta$ ) of the AZO pillars arrays system with 400 nm pitch and air host for three different measurement angles. At GBA wavelength, changes in both spectroscopic parameters can be seen. The blue shift in the GBA wavelength on increasing the incident angle is clearly evident here.

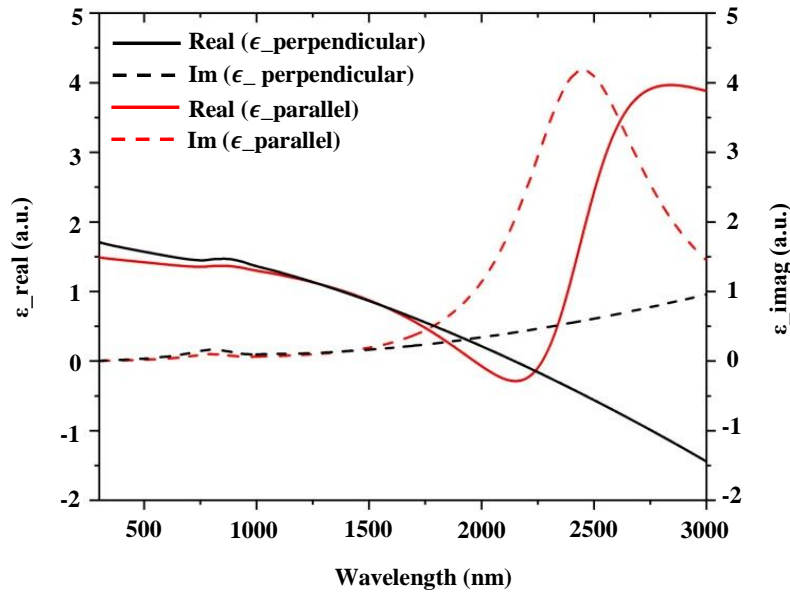


Figure 4: Theoretically calculated real and imaginary part of permittivity (epsilon,  $\epsilon$ ) of the AZO pillar structure with 400 nm pitch and air host, in parallel plane as well as in the perpendicular plane (along the semi-major axis of the pillar) is shown here. This numerical analysis is done by the transfer matrix method which is helpful to realize the cause of the GBA effect in this AZO pillar array structure.

From Figure 3(b), the particular wavelength at which the GBA effect is occurring can be sharply figured out by pointing out the wavelength at which  $\Delta$  (phase) is changing by 180 deg. The phase change of 180 deg is pointing out the complete phase shift by the system at that wavelength region giving rise to the Brewster phenomena for both polarizations. The comparison among all the GBA wavelengths for 35 deg, 40 deg and 45 deg is clearly indicating that the GBA wavelength shows a blue shift for higher incident angle as already seen in Figure 2. Figure 3(a) shows the variation of the parameter  $\Psi$  for this AZO structure for 35 deg, 40 deg, and 45 deg. At the GBA wavelength in each case (35 deg/40 deg/ 45 deg incident angle),  $\Psi$  goes from minimum to maximum or vice versa. Here the values of  $\Psi$  and  $\Delta$  at the GBA wavelength contributes to the  $r_p = -r_s$ , which leads to the GBA effect.

At this point, it is very clear that the AZO solid pillars array system with air as the host material has the GBA effect for both the 400 nm and 500 nm pitch. Now to understand the origin of this effect in this AZO pillar array structure, theoretical analysis has been conducted to see the optical behaviour of the structure by calculating the real and imaginary part of permittivity (epsilon,  $\epsilon$ ) in the plane of the pillar as well as along the direction of the pillar. The results are given in Figure 4. From the theoretical analysis shown in the figure 4 it is very clear that, the AZO pillar structure of 400 nm pitch and air host is anisotropic around 1500 nm which is the GBA wavelength of that structure measured from the reflection characteristics and the spectroscopic parameters. It is known that the anisotropic materials which can be considered as a type of metamaterial<sup>[39]</sup> have the potential to show GBA effect originated from the zero vector resultant radiation field in the reflection due to the total destructive interference of the magnetic and electric dipoles of the material at  $\theta_B^{s,p-pol}$ .<sup>[40-41]</sup>

To qualitatively understand the mechanism behind this phenomena one should focus on the behaviour of the electric dipoles of the media in presence of light. As the incident light interacts with the surface, the electric dipoles start oscillating at the interface between two media and then they re-radiate. It is a very well-known fact that the freely propagating light polarization is always perpendicular to the light propagation direction. Now the dipoles re-radiating at the interface produce the refracted or the transmitted light which oscillates in the same polarization direction of that light. These dipoles also create the reflected light but they do not radiate energy in the direction of the dipole moment. When the refracted light is p-polarized light and it propagates perpendicularly to the direction of the reflected light, the dipoles point along the specular reflection direction and therefore no light can be reflected. In this way, the Fresnel reflection coefficients for the incoming light vanish and the Brewster phenomenon takes place. For most of the materials this phenomena occurs only for p-polarized light. But here for this anisotropic AZO pillar array structure this is happening for both polarizations because of the equal strength of the electric permittivity and magnetic permeability at the GBA wavelength.

From the experimental reflection characteristics it is quite evident that these AZO pillar structures with air host showing the GBA effect are able to behave as the perfect light absorber at those particular wavelength and incident angle range. For the GBA and thus perfect light absorption property of these structures one may also use them as the ultrafast optical switches where incident angle and the operating wavelength can be used to switch from one optical state (ON state) to

the other optical (OFF state) state. Therefore, these AZO pillar array structures are expected to be useful for various conventional and novel scientific and technical applications in photonics.

**CONCLUSION:** We demonstrate here generalized Brewster angle effect in the NIR wavelength region using the array like structure of highly ordered high aspect ratio AZO solid nanopillars. The GBA wavelength depends on the incidence angle, pitch of the array structure along with the material composition. Here the AZO pillars were fabricated using a combination of advanced reactive ion etching technique and ALD technique. Experimental results are given to support the GBA effect of these anisotropic material and numerical investigations have been performed to elucidate the actual underlying cause of this effect. The tunable GBA effect along with several other advantages makes these structures useful for many applications including optical switches, perfect light absorbers, and protein sensing.

## **AUTHOR INFORMATION**

### **Corresponding Author**

\***E-mail:** gxs284@case.edu

### **Note**

The authors declare no competing financial interests.

### **Author Contributions**

S. C. performed optical characterization and wrote the manuscript. M.H. conducted the theoretical analysis of the structures. E. S. fabricated the samples. O. T. and A. V. L. contributed to the discussions of results and manuscript writing. G. S. Supervised the work. All authors have given approval to the final version of the manuscript.

## **ACKNOWLEDGEMENT**

This work was supported by Independent Research Fund Denmark, DFF Research Project 2 "PhotoHub" (8022-00387B) and NSF Grant (Award Number 1904592) - Instrument Development: Multiplex Sensory Interfaces Between Photonic Nanostructures and Thin Film Ionic Liquids. The authors would like to acknowledge the support from the National Centre for Nano Fabrication and Characterization (DTU Nanolab).

## **REFERENCES:**

- [1] Brewster, D., "On the laws which regulate the polarisation of light by reflexion from transparent bodies," *Philosophical Transactions of the Royal Society of London* 105, 125–159 (1815).
- [2] Lakhtakia, A., "Would Brewster recognize today's Brewster angle," *Optics News* 15, 14-18 (1989).
- [3] Sreekanth, K. V., ElKabbash, E., Medwal, R., Zhang, J., Letsou, T., Strangi, G., Hinczewski, M., Rawat, R. S., Guo, C., and Singh, R., "Generalized Brewster Angle Effect in Thin-Film Optical Absorbers and Its Application for Graphene Hydrogen Sensing," *ACS Photonics* 6, 1610-1617 (2019).
- [4] Chen, Z., Chen, X., Tao, L., Chen, K., Long, M., Liu, X., Yan, K., Stantchev, R. I., Pickwell-MacPherson, E., and Xu, J. B., "Graphene controlled Brewster angle device for ultra-broadband terahertz modulation," *Nat. Commun.* 9, 4909 (2018).

- [5] Hoenig, D., and Moebius, D., "Direct visualization of monolayers at the air–water interface by Brewster angle microscopy," *J. Phys. Chem.* 95, 4590-4592 (1991).
- [6] Kravets, V. G., Schedin, F., Jalil, R., Britnell, L., Gorbachev, R. V., Ansell, D.; Thackray, B., Novoselov, K. S., Geim, A. K., Kabashin, A. V., and Grigorenko, A. N., "Singular phase nano optics in plasmonic metamaterials for label-free single-molecule detection," *Nat. Mater.* 12, 304-309 (2013).
- [7] Giles, C. L., and Wild, W. J., "Brewster angles for magnetic media," *Int. J. Infrared Millimeter Waves* 6, 187-197 (1985).
- [8] Heading, J., "Generalized Investigations into the Brewster Angle," *Opt. Acta* 33, 755-770 (1986).
- [9] Giles, C. L., and Wild, W. J., "Brewster angles for magnetic media," *International Journal of Infrared and Millimeter Waves* 6, 187-197 (1985).
- [10] Paniagua-Domínguez, R., Feng, Y. Y., Miroshnichenko, A. E., Krivitsky, L. A., Fu, Y. H., Valuckas, V., and Gonzaga, L., "Generalized Brewster effect in dielectric metasurfaces," *Nat. Comm.* 7, 10362 (2016).
- [11] Tamayama, Y., Nakanishi, T., Sugiyama, K., and Kitano, M., "Observation of Brewster's effect for transverse-electric electromagnetic waves in metamaterials: Experiment and theory," *Phys. Rev. B: Condens. Matter Mater. Phys.* 73, 193104 (2006).
- [12] Tamayama, Y., "Brewster effect in metafilms composed of bi-anisotropic split-ring resonators," *Opt. Lett.* 40, 1382-1385 (2015).
- [13] Lakhtakia, A., "Would Brewster recognize today's Brewster angle," *Optics News* 15, 14-18 (1989).
- [14] Bassiri, S., Papas, C. H., and Engheta, N., "Electromagnetic wave propagation through a dielectric–chiral interface and through a chiral slab," *J. Opt. Soc. Am. A* 5, 1450-1459 (1988).
- [15] Mahlein, H. F., "Generalized Brewster-angle conditions for quarter-wave multilayers at non-normal incidence," *J. Opt. Soc. Am.* 64, 647-653 (1974).
- [16] Watanabe, R., Iwanaga, M., and Ishihara, T., "S-polarization Brewster's angle of stratified metal–dielectric metamaterial in optical regime," *Phys. Status Solidi B* 245, 2696-2701 (2008).
- [17] Lin, X., Shen, Y., Kaminer, I., Chen, H., and Soljacic, M., "Transverse-electric Brewster effect enabled by nonmagnetic two dimensional materials," *Phys. Rev. A: At., Mol., Opt. Phys.* 94, 023836 (2016).
- [18] Paniagua- Domínguez, R., Yu, Y. F., Miroshnichenko, A. E., Krivitsky, L. A., Fu, Y. H., Valuckas, V., Gonzaga, L., Toh, Y. T., Kay, A. Y. S., Luk'yanchuk, B., and Kuznetsov, A. I., "Generalized Brewster effect in dielectric metasurfaces," *Nat. Commun.* 7, 10362 (2016).
- [19] Shalaev, V. M., "Optical negative-index metamaterials," *Nat. Photonics* 1, 41-48 (2007).
- [20] Zheludev, N. I., "The road ahead for metamaterials," *Science* 328, 582-583 (2010).
- [21] Fu, C., Zhang, Z. M., and First, P. N., "Brewster angle with a negative index material," *Appl. Opt.* 44, 3716-3724 (2005).
- [22] Shkondin, E., Takayama, O., Panah, M. E. A., Liu, P., Larsen, P. V., Mar, M. D., Jensen, F., and Lavrinenko, A. V., "Large-scale high aspect ratio Al-doped ZnO nanopillars arrays as anisotropic metamaterials," *Optical Materials Express* 7, 1606-1627 (2017).
- [23] Lindroos, V., Tilli, M., Lehto, A., Motooka, T., and Veijola, T., "Handbook of silicon based MEMS materials and technologies," *Micro & Nano Technologies Series* 2010.
- [24] George, S., "Atomic layer deposition: an overview," *Chem. Rev.* 110, 111-131 (2010).

- [25] Takayama, O., Shkondin, E., Bogdanov, A., Aryaee Pahah, M. E., Golenitskii, K., Dmitriev, P. A., Repan, T., Malreanu, R., Belov, P., Jensen, F., and Lavrinenko, A. V., "Midinfrared surface waves on a high aspect ratio nanotrench platform," *ACS Photonics* 4, 2899-2907 (2017).
- [26] Takayama, O., Dmitriev, P., Shkondin, E., Yermakov, O., Panah, M. E. A., Golenitskii, K., Jensen, F., Bogdanov, A., and Lavrinenko, A. V., "Experimental Observation of Dyakonov Plasmons," *Semiconductors* 52, 442-446 (2018).
- [27] Shkondin, E., Repän, T., Aryaee Panah, M. E., Lavrinenko, A. V., and Takayama, O., "High Aspect Ratio Plasmonic Nanotrench Structures with Large Active Surface Area for Label-Free Mid-Infrared Molecular Absorption Sensing," *ACS Applied Nano Materials* 1, 1212-1218 (2018).
- [28] Shkondin, E., Repän, T., Takayama, O., and Lavrinenko, A. V., "High aspect ratio titanium nitride trench structures as plasmonic biosensor," *Optical Materials Express* 7, 4171-4182 (2017).
- [29] Shkondin, E., Takayama, O., Lindhard, J. M., Larsen, P. V., Mar, M. D., Jensen, F., and Lavrinenko, A. V., "Fabrication of high aspect ratio TiO<sub>2</sub> and Al<sub>2</sub>O<sub>3</sub> nanogratings by atomic layer deposition," *Journal of Vacuum Science & Technology A: Vacuum, Surfaces, and Films* 34, 031605, (2016).
- [30] Shkondin, E., Alimadadi, H., Takayama, O., Jensen, F., and Lavrinenko, A. V., "Fabrication of hollow coaxial Al<sub>2</sub>O<sub>3</sub>/ZnAl<sub>2</sub>O<sub>4</sub> high aspect ratio freestanding nanotubes based on the Kirkendall effect," *Journal of Vacuum Science & Technology A: Vacuum, Surfaces, and Films* 38, 013402 (2020).
- [31] Gnawali, R., Banerjee, P. P., Haus, J. W., Reshetnyak, V., and Evans, D. R., "Optical propagation through anisotropic metamaterials: Application to metallo-dielectric stacks," *Opt. Commun.* 425, 71-79 (2018).
- [32] Berreman, D. W., "Optics in stratified and anisotropic media: 4× 4-matrix formulation," *J. Opt. Soc. Amer.* 62, 502 (1972).
- [33] Shekhar, P., Atkinson, J., and Jacob, Z., "Hyperbolic metamaterials: fundamentals and applications," *Nano Convergence* 1, 14 (2014).
- [34] Garahan, A., Pilon, L., Yin, J., and Saxena, I., "Effective optical properties of absorbing nanoporous and nanocomposite thin films," *J. Appl. Phys.* 101, 014320 (2007).
- [35] Rakić, A. D., "Algorithm for the determination of intrinsic optical constants of metal films: application to aluminum," *Appl. Opt.* 34, 4755 (1995).
- [36] Wemple, S. H., and DiDomenico Jr, M., "Behavior of the electronic dielectric constant in covalent and ionic materials," *Phys. Rev. B* 3, 1338 (1971).
- [37] Gao, L., Lemarchand, F., and Lequime, M., "Exploitation of multiple incidences spectrometric measurements for thin film reverse engineering," *Opt. Express* 20, 15734 (2012).
- [38] Pierce, D. T., and Spicer, W. E., "Electronic structure of amorphous Si from photoemission and optical studies," *Phys. Rev. B* 5, 3017 (1972).
- [39] Agranovich, V. M., Shen, Y. R., Baughman, R. H., and Zakhidov, A. A., "Linear and nonlinear wave propagation in negative refraction metamaterials," *Phys. Rev. B* 69, 165112 (2004).
- [40] Paniagua-Dominguez, R., Yu, Y. F., Miroshnichenko, A. E., Krivitsky, L. A., Fu, Y. H., Valuckas, V., Gonzaga, L., Toh, Y. T., Kay, A. Y. S., Luk'yanchuk, B., and Kuznetsov, A. I. "Generalized Brewster effect in dielectric metasurfaces," *Nat. Comm.* 7, 10362 (2016).
- [41] Abujetas, D. R., Sánchez-Gil, J. A., and Sáenz, J. J., "Generalized Brewster effect in high-refractive-index nanorod-based metasurfaces," *Optics Express* 26, 31523 (2018).